

Nanoseconds molecular dynamics simulation of primary mechanical energy transfer steps in F₁-ATP synthase

Rainer A. Böckmann and Helmut Grubmüller

Theoretical Molecular Biophysics Group, Max-Planck-Institute for Biophysical Chemistry, Am Fassberg 11, 37077 Göttingen, Germany.

Published online: 11 February 2002, DOI: 10.1038/nsb760

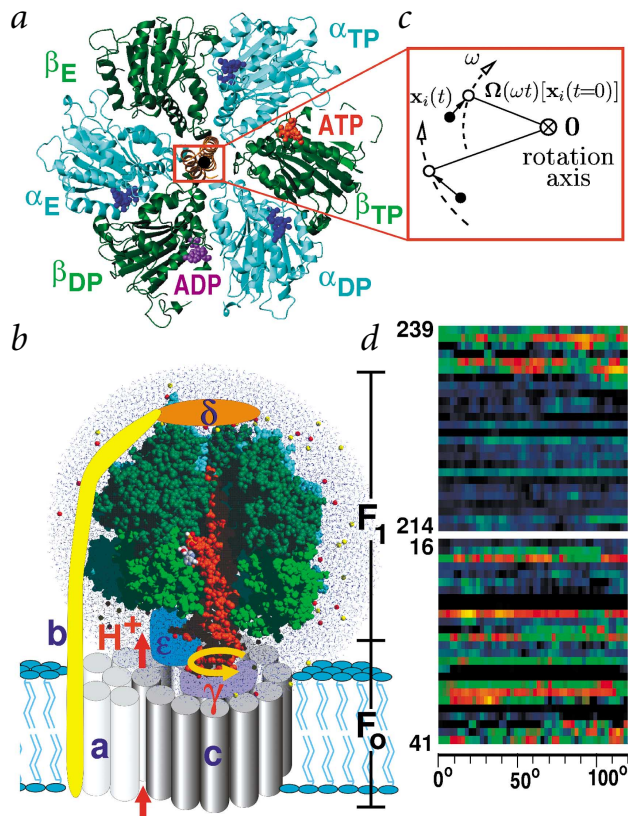
The mitochondrial membrane protein F_oF₁-ATP synthase synthesizes adenosine triphosphate (ATP), the universal currency of energy in the cell. This process involves mechanochemical energy transfer from a rotating asymmetric γ -'stalk' to the three active sites of the F₁ unit, which drives the bound ATP out of the binding pocket. Here, the primary structural changes associated with this energy transfer in F₁-ATP synthase were studied with multi-nanosecond molecular dynamics simulations. By forced rotation of the γ -stalk that mimics the effect of proton motive F_o-rotation during ATP synthesis, a time-resolved atomic model for the structural changes in the F₁ part in terms of propagating conformational motions is obtained. For these, different time scales are found, which allows the separation of nanosecond from microsecond conformational motions. In the simulations, rotation of the γ -stalk lowers the ATP affinity of the β_{TP} binding pocket and

triggers fast, spontaneous closure of the empty β_E subunit. The simulations explain several mutation studies and the reduced hydrolysis rate of γ -depleted F₁-ATPase.

F_oF₁-ATP synthase (Fig. 1a,b) utilizes the electrochemical potential of a transmembrane proton gradient to synthesize ATP^{1,2}. Notably, energy conversion involves mechanochemical energy transfer from a rotating asymmetric γ -'stalk' over a distance of >2.5 nm to the three ATP synthesis sites of the F₁ complex (Fig. 1a)³⁻⁵. X-ray structures of the F₁ unit^{6,7} show its three catalytic β -subunits in different conformational states, TP, DP and E, with bound ATP (analog), ADP and empty binding site, respectively⁶. The structures suggest that the energy consuming step in the ATP synthesis cycle — that is, ATP release — is driven by concerted conformational motions within the ($\alpha\beta$)₃ complex, which are dictated by the changing orientation of the asymmetric γ subunit inside ($\alpha\beta$)₃ (ref. 6), thus rendering F_oF₁-ATP synthase a 'molecular machine'.

The central metabolic role and high efficiency of this machine has triggered much experimental work on substrate-binding affinities⁸, thermodynamics, stoichiometry⁹ and kinetics⁸, as well as on mutants^{8,10,11} and crosslinks³. To combine these data into coherent pictures, several simplified models without incorporating atomic detail have been discussed^{10,12-16}. Here we study at the atomic level how these motions are induced by rotation of the γ -stalk, how and along which route they propagate towards the nucleotide binding sites, and why and in what sequence the observed structural changes lower ATP binding affinity at β_{TP} , as is required for ATP to leave the binding pocket after synthesis. Aiming at model-independent answers to these questions, we have performed molecular dynamics force probe simulations^{17,18} of the fully solvated ($\alpha\beta$)₃ γ complex (Fig. 1b), which is the minimal complex capable of normal ATPase activity^{19,20}. In the simulations, the lower part of the γ -stalk was forced to rotate (Fig. 1c)

Fig. 1 ATP synthase structure, function and simulation setup. **a**, A slice of F₁ at the level of the active sites, viewed from the cytosolic side. **b**, F_oF₁-ATP synthase with the atomically resolved F₁ simulation system. A proton flux through the membrane-bound F_o unit (red) drives rotation of the asymmetric γ -stalk (orange), with respect to the F₁ unit (green and cyan) located in the mitochondrial matrix. Co-rotation of F₁ is hindered by δ and b (yellow), the exact positioning of which is not generally agreed upon. This rotation triggers conformational changes mainly within the three β -subunits, DP, TP and E (green), which bind ADP and phosphate and subsequently drive ATP synthesis and release. These changes concern mostly the orientation of the lower-half of the β -subunit (light green), which can tilt with respect to the upper-half (dark green). Accordingly, the conformation seen for the empty subunit, β_E , is denoted 'open', whereas β_{TP} and β_{DP} are referred to as 'closed'⁶. After 120° rotation of γ , DP, TP and E switch roles clockwise. Our molecular dynamics simulations included the F₁ unit ($\alpha\beta$)₃ γ (except δ and b), bound nucleotides as shown in panel (a), a large solvation shell (blue) and salt ions (red and yellow), comprising a total of 183,674 atoms. **c**, In the simulations, torque was exerted onto the lower part of γ by subjecting the respective backbone atoms (filled circle) to restraining potentials (open circle), which are moved with constant angular velocity ω along concentric circles around the pseudo symmetry axis (circle with 'x') of the complex. Throughout the simulations, co-rotation of the ($\alpha\beta$)₃ complex was prevented by immobilizing the centers of mass of the putative δ contact region of two α -subunit head groups (residues α_{TP} 24–130 and α_{DP} 19–96), thereby mimicking the effect of the δ 'stator'. To prevent tilt of the whole system, the center of mass of residues α_E 255–265 and 310–320 were immobilized. **d**, The torque required to move the individual residues of γ within ($\alpha\beta$)₃ (black = zero or negative torque and yellow = 0.7×10^{-18} Nm) allows the identification of hot spots of mechanical energy transfer. Mainly due to Stokes' friction, the averaged torque is larger by a factor of ~50 than the measured average torque of 5×10^{-20} Nm (ref. 22). Comparison of that value with the value of 1.02×10^{-18} Nm obtained from an additional simulation with four-fold lower angular velocity ($\omega = 29^\circ \text{ ns}^{-1}$) yields a velocity-dependent frictional torque contribution of $(2.0 \pm 0.3) \times 10^{-18}$ Nm. The associated dissipated energy raises the temperature of the γ -subunit by <1 K.



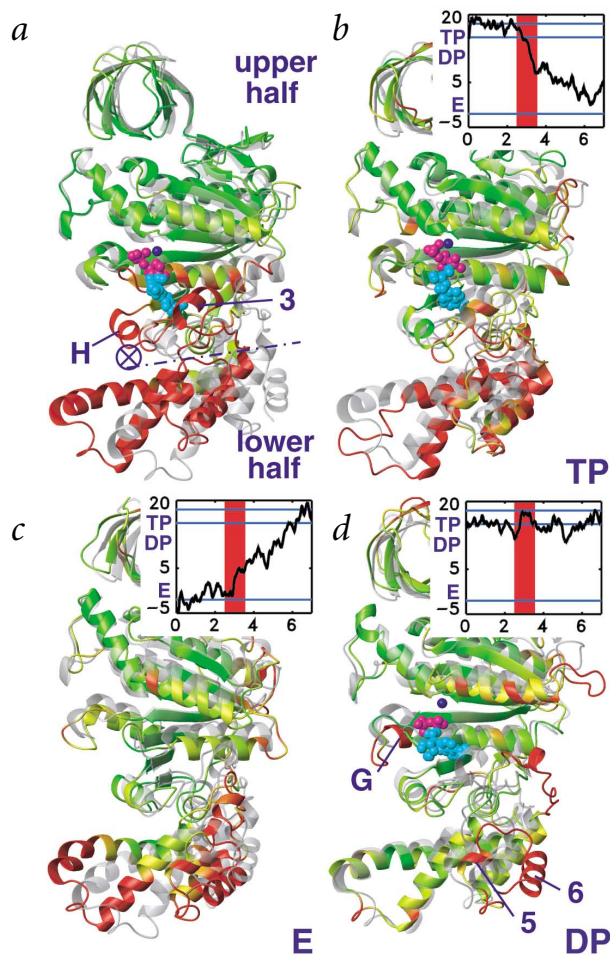


Fig. 2 Structural changes of the β -subunits induced by enforced rotation of the γ -stalk. The size of these changes is color-coded (green = small and red = large). **a**, Overlay of β_{TP} (colored) and β_E -subunits (gray,) taken from the X-ray structure, in closed and open conformation, respectively (rotation axis = circle with 'x'). **b-d**, Changes in β_{TP} , β_E and β_{DP} , respectively, as induced by enforced 120° rotation and subsequent free dynamics. Shown are the initial (X-ray) structures (gray) and final structures (colored). The insets show the rotation angle between upper and lower part of the respective β -subunits in the course of the 7 ns simulation. The red bar indicates the period of enforced rotation, and green lines denote the three β -subunit angles of the equilibrated X-ray structure.

of $\omega = 115^\circ \text{ ns}^{-1}$ (Fig. 1c). During a subsequent relaxation period of 3.5 ns, within which the lower part of the γ -subunit was kept restrained to avoid back-rotation, the induced conformational motions propagated further towards the active sites. The torques exerted onto the individual γ -residues during the 120° forced rotation (Fig. 1d) show peaks, reflecting energy transfer to $(\alpha\beta)_3$, dissipation and enforced crossing of associated energy barriers. This crossing is largely nonactivated at the nanosecond simulation time scale; therefore, the peaks should be more pronounced in our torque profiles than they would appear at physiological turnover rates.

Most of the C-terminal γ -helix (residues 214–233) rotates almost freely. Residues 234–238, which form the middle part of the γ -stalk and are located close to the DELSEED region of the β_{TP} subunit, exhibit larger torques mainly due to steric interactions, which bend away the helix-coil(DELSEED)-helix region of β_{TP} . For the reverse ATPase direction, this implies considerable energy transfer from the ATP-loaded β -subunit to γ , in agreement with accepted models^{10,12–16}. For the N-terminal γ -helix, the apparent torque peak at 30° for Arg 36 is caused by the rupture of a hydrogen bonding network between γ (residues Lys 30, Arg 33 and Arg 36) and Asp 409 from α_E , as well as the β_E -DELSEED region. Here the entire load apparently rests on the lowermost γ -residues, Arg 36 and Glu 35, due to the intrinsic elasticity of the γ -helix. Steric interactions also occur, mainly between Met 25 and the γ -proximal part of helix 1 (Fig. 4), giving rise to the second pronounced peak. For Lys 18, water bridges cause moderate forces. The breaking of hydrogen bonds between γ (Arg 228) and β_{DP} (Glu 395) at 50° is not seen in the torque profiles.

Opening and closing motions

Major changes are seen in two of the three β -subunits during enforced rotation and subsequent free dynamics (Fig. 2). The lower part of β_{TP} is pushed sideways toward α_{DP} and downward toward an open configuration (Fig. 2b). This observation is quantified by the change of the bending angle (Fig. 2, inset) between the two domains separated by the dashed line in Fig. 2a, which approaches that seen in β_E . Simultaneously, an upwards rotation of the lower half of β_E towards the closed X-ray conformation of β_{TP} and β_{DP} is observed (Fig. 2c). Initially, this motion is sterically obstructed by both the γ -subunit and β_{TP} and, therefore, proceeds synchronously to the removal of these obstacles. Although this motion proceeds very fast, it is apparently not driven by the γ -rotation, in contrast to the motion in β_{TP} . In this sense, this spontaneous motion resembles the relaxation of a spring. In particular, substrate binding is not required. In confirmation, β_{TP} (including bound substrate) remained closed in additional simulations of isolated solvated β -subunits, whereas β_E closed spontaneously within 3 ns (data not shown). These findings imply that, for the reverse hydrolysis cycle, opening of β_E is an energy-consuming step that is driven, *via* γ -rotation, by

to mimic the F_0 rotation caused *in vivo* by the proton motive force; the results reveal the subsequent conformational motions triggered from this rotation.

Due to the huge computational cost of such simulations, the time span covered is limited to several nanoseconds — that is, considerably shorter than the microseconds time scale at which these conformational motions presumably take place *in vivo*²¹. Accordingly, torques larger than the measured ones²² by factors of 12 and 50 had to be applied in the simulations. Furthermore, slow (microsecond) conformational motions are unlikely to show up. For the faster motions that are seen in the simulations, however, the large amount of available experimental data allowed us to verify that these motions are described correctly.

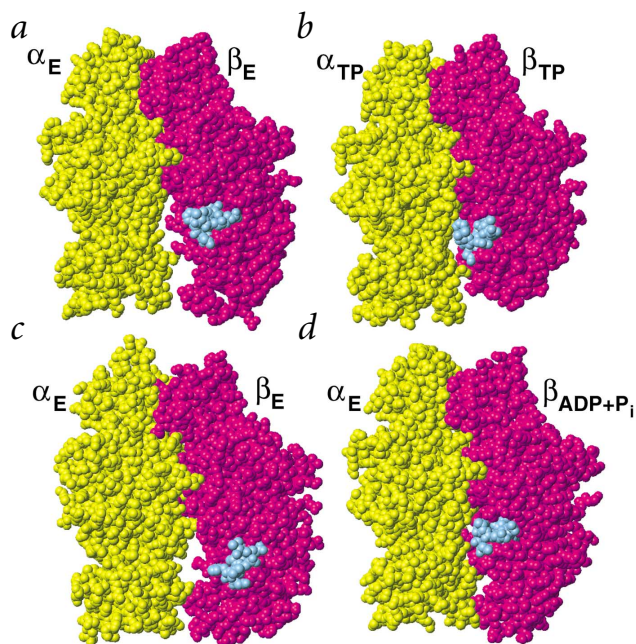
Forced 120° rotation of the γ -subunit

During an initial equilibration phase, the system remained close to the X-ray structure. In particular, the hydrogen bonding networks between the nucleotides and the residues of the respective binding pockets remained intact, and the Mg^{2+} coordination, as well as ligated water molecules, displayed the main features of the X-ray model²³. Furthermore, the fluctuations of the individual binding pocket residues during equilibration agree well with those obtained from the averaged temperature factors eight other X-ray structures of ATPase (PDB entries 1BMF, 1E79, 1COW, 1E1Q, 1E1R, 1EFR, 1H8H and 1NBM), with correlation coefficients of 0.84, 0.68 and 0.70 for the empty, ATP and ADP pocket, respectively.

After equilibration, a 120° force probe rotation simulation in the synthesis direction was carried out with an angular velocity



Fig. 3 Changes at the catalytic α - β interface. Helix 3 (residues 418–426) of each β -subunit is highlighted in blue. **a**, Open empty and **b**, closed TP conformation, as seen in the X-ray structure that has been used as starting structure for the simulations. **c**, α_E - β_E interface from the simulation after enforced γ -rotation and equilibration. **d**, A recent half-closed structure with bound ADP and sulfate, which has been proposed as an intermediate²⁴.



conformational motions of one or both of the other β -subunits — either by ATP binding or by phosphate release¹⁶. Without γ -coupling, β_E would likely get trapped in closed conformation. Indeed, the hydrolysis rate of γ -depleted $(\alpha\beta)_3$ is drastically reduced²⁰.

Significantly smaller changes are seen for β_{DP} (Fig. 2*d*), where the orientation of the lower part is nearly unchanged. Exceptions to this are helices 5 and 6, which bend slightly outwards, as well as the γ -proximal part of helix G. For all three β -subunits, considerable fluctuations are seen for the short helix 3 at the adenine pocket, residues 418–426, in agreement with the disorder seen for these residues in the β_E X-ray structure. Overall, the opening and closing motions of the lower halves of the β -subunits are nearly completed within the 7 ns simulation time span, without being subjected to any restraining potential. Apparently, the frictional forces are weak enough to allow even the observed large motions of the lower β -halves within nanoseconds.

Despite the spontaneous closure of the β_E subunit, the α_E - β_E catalytic interface remains open. This can be seen by comparing the positions of helix 3 (Fig. 3, blue) for the open α_E - β_E (Fig. 3*a*) and the closed α_{TP} - β_{TP} (Fig. 3*b*) catalytic interfaces from the crystal structure, with the respective position seen after enforced rotation for β_E (Fig. 3*c*). Comparing the structure with the recently solved half-closed β_{ADP+Pi} conformation²⁴ (Fig. 3*d*) is also instructive. Here, the catalytic interface is closed even though the β -subunit adopts an open conformation similar to the β_E subunit (Fig. 3*a*). Comparison of the X-ray structures of β_E and β_{ADP+Pi} reveals a rotation of the C-terminal domain around the axis of the $(\alpha\beta)_3$ subcomplex, approximately perpendicular to the rotation axis that connects the open with the closed conformation²⁴. A similar ‘sideways bending’, in reverse direction, is seen in our simulation for the lower half of the β_{TP} subunit, which is driven here by the forced γ -rotation in the synthesis direction. In contrast to the half-closed crystal structure, which was interpreted as a hydrolysis intermediate before ADP release²⁴, the spontaneously closed β_E subunit probably resembles a synthesis intermediate before ADP binding.

Triggered sequence of conformational changes

Next, we analyzed the details and timing of the conformational motions in β_{TP} (Fig. 4), which are triggered by γ -subunit rotation. Overall, a domino-like propagation of structural changes towards the ATP-binding site is observed, which proceeds much slower than an elastic wave and just below the velocity at which frictional forces in proteins are found to become dominant^{17,18,25}. Accordingly, friction should be negligible at physiological time scales, in agreement with the ~100% efficiency of the enzyme¹⁴.

Closer inspection reveals that the structural changes propagate along two main routes toward the ATP-binding site and, therefore, are expected to affect the energy transfer required for the decrease in ATP binding affinity. The dominant route (red, Fig. 4) leads *via* the DELSEED region and the adjacent helices 1 and 2, as well as *via* the β_{TP} hinge region (residues 136–144 and 354–359), toward the binding pocket. Here, three steps can be distinguished. Almost synchronously with the γ -rotation, the γ -proximal part of helix 1 and, subsequently helix 2, are pushed

downward and sideways. This motion is dominated by steric interactions, which is consistent with the observation that the generated torque is nearly unaffected in mutants with decreased negative charge in the highly charged DELSEED region¹¹. These motions drive a second step, during which the more distal parts of helices 1 and 2 start to move. At this time, the hinge region undergoes complex structural changes. In a third step, these changes drive helix B, which is located at the binding site, outward as it becomes more tilted with respect to helix C. The second, less pronounced route of structural changes (green, Fig. 4) involves the hydrophobic bearing (residues 273–281) of γ (region E) and region G (Fig. 4). These are pushed sideways by γ , such that hydrogen bonds between β_{TP} Asp 315 and Asp 316 to γ Arg 252 are formed. Subsequently, helix H is pushed slightly downward, and the two strands of β -sheet 7 start to disrupt. Presumably, these motions also contribute to shifting helix B outward.

As with the overall tilting motion of the lower half of β_{TP} , the more detailed structural changes described above also depart from the β_{TP} X-ray structure and approach the open β_E X-ray conformation, as can be seen by comparing the root mean square (r.m.s.) distances of the respective β_{TP} regions before and after γ -rotation to the β_E X-ray structure. For helix H, a drop from 0.34 nm to 0.25 nm is observed; for the two strands of β -sheet 7, the drop is from 0.15 nm to 0.13 nm. The tilt angle between helices B and C increases from 25° to 38°, approaching more than half way that of β_E (47°).

Further conformational changes are expected from comparison of the β_{TP} subunit after forced rotation with the X-ray β_E -structure; however, these changes are not (yet) seen in the simulations. Therefore, these motions (blue, Fig. 4) probably occur at slower time scales and/or are triggered by ATP release. They include further tilting of helix B, completion of the downward motion of helices 1 and 2, and significant motion of helix H. Closer analysis of the structural changes leads us to speculate that rotation of the lower half is completed only after ATP release, which should then trigger the motion of helix H. This agrees with the finding that for β_E , the expected reverse motion of helix H is not seen in the simulations and, hence, is also probably

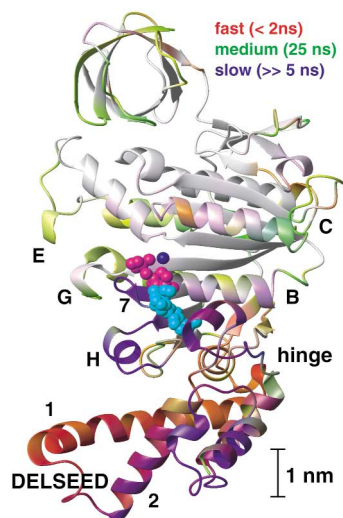


Fig. 4 Sequence and timing of conformational changes in β_{TP} . Shown are fast changes that mainly occur during forced rotation (red), slower ones that mainly occur during the subsequent free dynamics (yellow and green) and those not observed in the 7 ns simulation (blue) but are evident from the differences to the β_E X-ray structure. No significant changes are seen for the gray regions. The labels denote α -helices, β -strands and regions referred to in the text.

which is important for intercatalytic-site cooperativity¹⁰, moves towards the position seen in β_E , and a transient hydrogen bond is formed between β_{TP} Asp 386 and α_{DP} Arg 398. Overall, γ -rotation is found to decrease the number of α_{DP} - β_{DP} and α_{DP} - β_{TP} van der Waals contacts.

Conclusions and implications

Our molecular dynamics simulations of forced γ -rotation suggest a sequence of structural changes that effect primary mechanochemical energy transfer steps within F_1 -ATP synthase. Many structural changes that are expected from the three X-ray intermediates are correctly reproduced. Because none of these motions have been artificially directed towards the expected target structure, the agreement shows that the necessarily accelerated rotation of the γ -stalk does not severely change their character.

In contrast to previous interpolations between the three known intermediates, the simulations provide a causal picture of a sequence of structural motions, with one triggering the next. Already within the simulation time span of 7 ns, the structural changes proceed sufficiently far enough to transfer a significant amount of energy to the β_{TP} -binding site, as estimated from its decreased ATP-binding affinity. This decrease is affected gradually by sequential and well-concerted retraction of three charged Arg residues from the bound ATP. Two main conformational energy transfer routes have been identified that couple γ -rotation to this retraction. Unexpectedly, a fast spontaneous closure of the empty β -subunit is seen during γ -rotation.

Some of the expected structural changes are not seen in the simulations and, therefore, probably occur at slower time scales than those accessible to our simulations. This finding allows classification of the structural changes into fast (nanoseconds) and slow changes. Necessarily, many questions remain open but can now be addressed in subsequent studies — for example, concerning the conformational changes triggered by ATP removal, ATP binding, ATP synthesis or phosphate binding, and concerning the specific role of the α -subunits.

triggered by ADP/phosphate binding. Following the suggestion that the ATP concentration-independent delay of the γ -rotation after the recently observed 90° substep of the hydrolysis cycle is defined by ATP+P_i release²¹, which, in turn, is tied to internal conformational motions, one may further speculate that these are among the slow motions not seen in our simulations.

Induced binding site changes reduce ATP binding affinity

Focusing at the catalytic ATP-binding site (Fig. 5), a sequential retraction of residues β Arg 191, α Arg 373 and β Arg 189 from ATP is seen, which is quantified by the respective distance changes (blue, Fig. 5, inset). This sequence is initiated, immediately after γ -rotation, by a 0.5 nm shift of β Arg 191 towards α_{TP} , which forms a new hydrogen bond to α Gln 163, thereby weakening its interaction to ATP. Subsequently, initially strong hydrogen bonds (dashed lines, Fig. 5) between ATP and residues α Arg 373 and β Arg 189 rupture, further decreasing ATP binding affinity. These two residues are essential for the promotion of rotational multisite catalysis^{26–28}. We suggest β Arg 191 as a further target for mutation studies.

Simultaneous to the first hydrogen bond rupture, the coordination of Thr 163 (green, Fig. 5) to the magnesium ion is lost. The whole process is compatible with the ‘zipper-model’¹⁶, which postulates a sequential rupture of hydrogen bonds between ATP and the binding pocket. Assuming that changes of ATP binding affinity are dominated by the interaction between ATP and the binding pocket, a continuous ATP affinity decrease of β_{TP} can be inferred from the increasing interaction energy estimate between ATP and the binding pocket (black curve, Fig. 5, inset) as the net effect of the observed structural changes.

Also seen are changes at the α - β interfaces, which might contribute to the observed binding cooperativity⁸. In particular, with a delay of 2 ns after rotation of the γ -stalk, β_{TP} Arg 260,

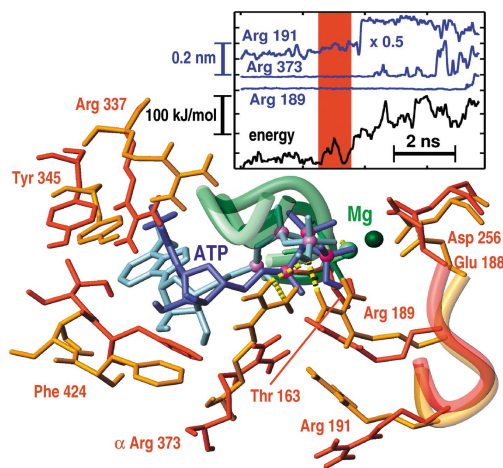


Fig. 5 Changes at the β_{TP} ATP binding site after the 120° rotation and free dynamics. Shown are selected residues involved in ATP binding before (yellow, with ATP in light blue) and after enforced rotation and subsequent free dynamics (red, with ATP in blue). The backbones of part of the P-loop (Ala 158–Val 164) and of Glu 188–Glu 192 are colored green and orange, respectively. Residue numbers refer to β_{TP} if not annotated otherwise. The inset shows distances (blue) between the donor nitrogen atoms of three Arg residues involved in ATP binding and the respective ATP phosphates (reduced scale for Arg 191), as well as an estimate (black) for the change in interaction energy between ATP and the binding pocket in the course of the simulation. The period of enforced rotation is highlighted red.



Methods

Molecular dynamics simulations. All molecular dynamics simulations were carried out with the parallel MD program EGO²⁹, the CHARMM force field³⁰, a 1 fs integration step size and efficient computation of the full Coulomb interaction³¹ ($\epsilon = 1$). Nonpolar hydrogen atoms were described by compound atoms³⁰, and the lengths of chemical bonds to hydrogen atoms were fixed. All surface water molecules were subjected to 'deformable boundary forces'^{30,29} and coupled to a 300 K heat bath through stochastic forces (coupling constant $\beta = 10 \text{ ps}^{-1}$). All other atoms were weakly coupled to a heat bath ($\beta = 1 \text{ ps}^{-1}$) via velocity rescaling. Mainly, 32 Power3 processors of an IBM RS/6000 SP3 parallel computer were used, totaling ~280,000 h of cpu time.

System setup. The $(\alpha\beta)_3\gamma$ X-ray structure of F₁-ATPase from bovine heart mitochondria⁶ (Protein Data Bank entry 1BMF) was used. A structure with completely resolved γ -, δ - and ϵ -subunits is available⁷ but shows a shift of the γ -subunit relative to $(\alpha\beta)_3$. That shift is attributed to lattice contacts in the F₁ crystals⁷, presumably entailing distortions in the α_{TP} -, β_E - and α_E -subunits and shifting the guanidinium group of α_{TP} Arg 373 in the active site⁷, which is important for cooperativity^{26,27}. We do not expect the lack of the δ - and ϵ -subunits and of part of the γ -subunit to affect our results, because these parts do not contact the $(\alpha\beta)_3$ -part (except for one hydrogen bond between γ and β_{DP}). A third structure²⁴ has recently become available; however, β_E is in an intermediate conformation and, therefore, not considered an appropriate start structure. The 1BMF structure was surrounded by 51,788 TIP3 water molecules³² and 297 ions (Na⁺ and Cl⁻) at physiological concentration determined using SOLVATE²⁹. For the placement of water molecules, energetic and steric criteria were used²⁹. A nonspherical solvent volume with a minimum surface distance to the enzyme of 1.2 nm was chosen.

Equilibration. After 30,000 minimization steps, the system was equilibrated for 2.47 ns, and the heavy atom r.m.s. deviations from the X-ray structure were monitored. The overall r.m.s. deviation showed the usual fast increase to 0.2 nm during the first 200 ps and a slow drift for the subsequent 2 ns; it stabilized at 0.27 nm. The r.m.s. deviation of the ADP, ATP and empty binding sites were already stabilized after 1.0 ns at 0.2 nm, 0.13 nm and 0.22 nm, respectively. The binding sites were defined as those residues which form hydrogen bonds or water bridges to the substrate, or are located close to the substrate — that is, α_{343} , 344, 349 and 368–373, and β_{158} –164, 188–192, 256, 257, 260, 337, 345, 416, 418, 421, 424 and 425. The only significant change seen is a move of ADP further into the binding pocket, such that the adjacent Phe 424 from β_{DP} becomes more flexible. A missing ion not resolved in the X-ray structure probably causes this motion. The lower half of β_E tilted slightly towards the γ -stalk, forming a new hydrogen bond.

Force probe simulations. Torque was exerted onto the lower part of γ (Fig. 1c). The n backbone atoms of residues 16–41 and 214–239 with positions x_i were subjected to a rotating potential, $V = \frac{1}{2}k \sum_{i=1}^n [\Omega(\omega t)x_i(t=0) - x_i(t)]^2$. The rotation matrix Ω moved the minima of V along concentric circles around the symmetry axis of the complex. A stiff spring coefficient of $k = 7 \text{ N m}^{-1}$ has been used. The torques $\Theta_i(t)$ exerted on the individual atoms were computed from the deflection of the actual atomic positions $x_i(t)$ from their respective minima, $\Theta_i(t) = \Omega(\omega t)x_i(t=0) \times k[\Omega(\omega t)x_i(t=0) - x_i(t)]$. Torque profiles per residue were obtained from the summed atomic torques, averaged over 50 ps intervals.

Post-simulation analysis. The change of interaction energy between the β_{TP} binding pocket and ATP was estimated from the sum of the van der Waals and the Coulomb interactions between ATP and all binding pocket atoms within a 0.8 nm vicinity. Focusing at timing rather than accurate energies, $\epsilon = 5$ was used as a rough description of dielectric screening. The timing of the motion of each β_{TP} -residue was characterized by its relative average location $\langle (x_e - x_s)(x(t) - x_s) / |x_e - x_s|^2 \rangle_t$ in configurational space along the distance vector connecting the equilibrated start configuration x_s ($t = 2.5 \text{ ns}$) and a final configuration x_e ($t = 6.78 \text{ ns}$). The size of structural motions was quantified via r.m.s. distances between the structure averaged over the last nanosecond of the simulation and the X-ray structure. Figures were created with MOLMOL³³ (Figs. 1a, 2–4) and RASMOL³⁴ (Fig. 1b).

Acknowledgments

We thank W. Junge, A. Engel, B. de Groot, B. Heymann, K. Schulten, W. Allison, D. Chandler, V. Helms, M. Hofmann, K. Kinoshita, V. Knecht, R. Lang, G. Oster, G. Schröder and H. Wang for stimulating discussions and for critical reading of the manuscript; B. de Groot for help with the GROMACS program package; and G. Schneider and O. Haan for their support. Computer time was provided by the Göttingen computer center (GWDG) and the Paderborn center for parallel computing (PC²).

Competing interests statement

The authors declare that they have no competing financial interests.

Correspondence should be addressed to H.G. email: hgrubmu@gwdg.de

Received 1 November, 2001; accepted 21 December, 2001.

- Mitchell, P. *Nature* **191**, 144–148 (1961).
- Boyer, P.D. *Biochim. Biophys. Acta* **1140**, 215–250 (1993).
- Duncan, T.M., Bulygin, V.V., Zhou, Y., Hutcheon, M.L. & Cross, R.L. *Proc. Natl. Acad. Sci. USA* **92**, 10964–10968 (1995).
- Sabbert, D., Engelbrecht, S. & Junge, W. *Nature* **381**, 623–625 (1996).
- Noji, H., Yasuda, R., Yoshida, M. & Kinoshita, K. *Nature* **386**, 299–302 (1997).
- Abrahams, J.P., Leslie, A.G.W., Lutter, L. & Walker, J.E. *Nature* **370**, 621–628 (1994).
- Gibbons, C., Montgomery, M.G., Leslie, A.G.W. & Walker, J.E. *Nature Struct. Biol.* **7**, 1055–1061 (2000).
- Weber, J. & Senior, A.E. *Biochim. Biophys. Acta* **1319**, 19–58 (1997).
- Pänke, O. & Rumberg, B. *Biochim. Biophys. Acta* **1322**, 183–194 (1997).
- Ren, G. & Allison, W.S. *Biochim. Biophys. Acta* **1458**, 221–233 (2000).
- Hara, K.Y. et al. *J. Biol. Chem.* **275**, 14260–14263 (2000).
- Boyer, P.D. *Annu. Rev. Biochem.* **66**, 717–749 (1997).
- Engelbrecht, S. & Junge, W. *FEBS Lett.* **414**, 485–491 (1997).
- Cherepanov, D.A., Mulikidjanian, A.Y. & Junge, W. *FEBS Lett.* **449**, 1–6 (1999).
- Weber, J., Nadanaciva, S. & Senior, A.E. *FEBS Lett.* **483**, 1–5 (2000).
- Oster, G. & Wang, H.Y. *Biochim. Biophys. Acta* **1458**, 482–510 (2000).
- Grubmüller, H., Heymann, B. & Tavan, P. *Science* **271**, 997–999 (1996).
- Izrailev, S., Stepaniants, S., Balsara, M., Oono, Y. & Schulten, K. *Biophys. J.* **72**, 1568–1581 (1997).
- Dunn, S.D. & Futai, M. *J. Biol. Chem.* **255**, 113–118 (1980).
- Miwa, K. & Yoshida, M. *Proc. Natl. Acad. Sci. USA* **86**, 6484–6487 (1989).
- Yasuda, R., Noji, H., Yoshida, M., Kinoshita, K. & Itoh, H. *Nature* **410**, 898–904 (2001).
- Pänke, O., Cherepanov, D.A., Gumbiowski, K., Engelbrecht, S. & Junge, W. *Biophys. J.* **81**, 1220–1233 (2001).
- Weber, J., Hammond, S.T., Wilke-Mounts, S. & Senior, A.E. *Biochemistry* **37**, 608–614 (1998).
- Menz, R.I., Walker, J.E. & Leslie, A.G.W. *Cell* **106**, 331 (2001).
- Heymann, B. & Grubmüller, H. *Chem. Phys. Lett.* **303**, 1–9 (1999).
- Nadanaciva, S., Weber, J., Wilke-Mounts, S. & Senior, A.E. *Biochemistry* **38**, 15493–15499 (1999).
- Le, N.P. et al. *Biochemistry* **39**, 2778–2783 (2000).
- Nadanaciva, S., Weber, J. & Senior, A.E. *Biochemistry* **38**, 7670–7677 (1999).
- Eichinger, M., Heller, H. & Grubmüller, H. In *Workshop on molecular dynamics on parallel computers* (eds Esser, R. et al.) 154–174 (World Scientific, Singapore; 2000).
- Brooks, B.R. et al. *J. Comp. Chem.* **4**, 187–217 (1983).
- Eichinger, M., Grubmüller, H., Heller, H. & Tavan, P. *J. Comp. Chem.* **18**, 1729–1749 (1997).
- Jorgensen, W.L., Chandrasekhar, J. & Madura, J.D. *J. Chem. Phys.* **79**, 926–935 (1983).
- Koradi, R., Billeter, M., & Wüthrich, K. *J. Mol. Graphics* **14**, 51–55 (1996).
- Sayle, R.A. & Milnerwhite, E.J. *Trends Biochem. Sci.* **20**, 374–376 (1995).